Molecular Genetics and Metabolism Reports 35 (2023) 100967

Contents lists available at ScienceDirect

Molecular Genetics and Metabolism Reports

journal homepage: www.elsevier.com/locate/ymgmr

Exogenous aralar/slc25a12 can replace citrin/slc25a13 as malate aspartate shuttle component in liver

Luis González-Moreno [a,b,c], Andrea Santamaría-Cano [a,b,c], Alberto Paradela [d], María Luz Martínez-Chantar [e,f], Miguel Á. Martín [g,h,r], Mercedes Pérez-Carreras [i], Alberto García-Picazo [j], Jesús Vázquez [k,l], Enrique Calvo [k,l], Gloria González-Aseguinolaza [m,n], Takeyori Saheki [o], Araceli del Arco [b,c,p,q], Jorgina Satrústegui [a,b,c], Laura Contreras [a,b,c,*]

[a] Departamento de Biología Molecular, Universidad Autónoma de Madrid, 28049 Madrid, Spain
[b] Instituto Universitario de Biología Molecular, (IUBM), and Centro de Biología Molecular Severo Ochoa, Universidad Autónoma de Madrid, Madrid, Spain
[c] Instituto de Investigaciones Sanitarias Fundación Jiménez Díaz (IIS-FJD), Universidad Autónoma de Madrid, 28049 Madrid, Spain
[d] Centro Nacional de Biotecnología (CNB), CSIC. C/Darwin 3, 28049 Madrid, Spain
[e] Liver Disease Lab, CIC bioGUNE, Basque Research and Technology Alliance (BRTA), 48160 Derio, Bizkaia, Spain
[f] Centro de Investigación Biomédica en Red de Enfermedades Hepáticas y Digestivas (CIBERehd), Instituto de Salud Carlos III, 28029 Madrid, Spain
[g] Grupo Enfermedades Mitocondriales y Neuromusculares, Instituto de Investigación Hospital 12 de Octubre (imas12), Madrid, Spain
[h] Servicio de Genética, Hospital Universitario 12 de Octubre, Madrid, Spain
[i] Servicio del Aparato Digestivo, Hospital Universitario 12 de Octubre, Madrid, Spain
[j] Departamento de Cirugía General Aparato Digestivo, Hospital Universitario 12 de Octubre, Madrid, Spain
[k] Centro Nacional de Investigaciones Cardiovasculares (CNIC), Madrid, Spain
[l] CIBER de Enfermedades Cardiovasculares (CIBERCV), Madrid, Spain
[m] Gene Therapy and Regulation of Gene Expression Program, Center for Applied Medical Research (CIMA), University of Navarra, 31008 Pamplona, Spain
[n] IdiSNA Navarra Institute for Health Research, 31008 Pamplona, Spain
[o] Ito Memorial Hospital, Ibusuki City, Japan
[p] Facultad de Ciencias Ambientales y Bioquímica, Universidad de Castilla la Mancha, Toledo 45071, Spain
[q] Centro Regional de Investigaciones Biomédicas, Unidad Asociada de Biomedicina, Toledo 45071, Spain
[r] Centro de Investigación Biomédica en Red de Enfermedades Raras (CIBERER), ISCIII, Madrid, Spain

ARTICLE INFO

Keywords:
Mitochondria
Citrin deficiency
Aspartate-glutamate carrier
Malate-aspartate shuttle
Hepatocyte

ABSTRACT

The deficiency of CITRIN, the liver mitochondrial aspartate–glutamate carrier (AGC), is the cause of four human clinical phenotypes, neonatal intrahepatic cholestasis caused by CITRIN deficiency (NICCD), silent period, failure to thrive and dyslipidemia caused by CITRIN deficiency (FTTDCD), and citrullinemia type II (CTLN2). Clinical symptoms can be traced back to disruption of the malate-aspartate shuttle due to the lack of citrin. A potential therapy for this condition is the expression of aralar, the AGC present in brain, to replace citrin. To explore this possibility we have first verified that the NADH/NAD^+ ratio increases in hepatocytes from *citrin(−/−)* mice, and then found that exogenous aralar expression reversed the increase in NADH/NAD^+ observed in these cells. Liver mitochondria from *citrin (−/−)* mice expressing liver specific transgenic aralar had a small (~ 4–6 nmoles x mg $prot^{-1}$ x min^{-1}) but consistent increase in malate aspartate shuttle (MAS) activity over that of *citrin(−/−)* mice. These results support the functional replacement between AGCs in the liver. To explore the significance of AGC replacement in human therapy we studied the relative levels of citrin and aralar in mouse and human liver through absolute quantification proteomics. We report that mouse liver has relatively high aralar levels (citrin/aralar molar ratio of 7.8), whereas human liver is virtually devoid of aralar (CITRIN/ARALAR ratio of 397). This

Abbreviations: AQUA, Absolute Quantification methods; AGC, aspartate-glutamate carrier; (BNGE), Blue native gel electrophoresis; CD, CITRIN Deficiency; CTNL2, citrullinemia type II; DAB, 3,3-diaminobenzidine; FBS, Fetal Bovine serum; FTTDCD, failure to thrive and dyslipidemia caused by CITRIN Deficiency; GOT, aspartate transaminase; GPD2, mitochondrial glycerol phosphate dehydrogenase; GPS, glycerol phosphate shuttle; hCitrin, human citrin; IM, imaging medium; LC-MS, liquid chromatography mass spectrometry; LNP, lipid nanoparticles; MAS, malate aspartate shuttle; NAA, N-Acetyl-aspartate; NICCD, neonatal intrahepatic cholestasis caused by CITRIN Deficiency; OXPHOS, oxidative phosphorylation; PRM, parallel reaction monitoring; PFA, paraformaldehyde; SDS, sodium dodecyl sulfate; TBS, Tris-Buffered saline..

* Corresponding author.
E-mail address: lcontreras@cbm.csic.es (L. Contreras).

https://doi.org/10.1016/j.ymgmr.2023.100967
Received 9 March 2023; Accepted 10 March 2023

large difference in endogenous aralar levels partly explains the high residual MAS activity in liver of *citrin(−/−)* mice and why they fail to recapitulate the human disease, but supports the benefit of increasing aralar expression to improve the redox balance capacity of human liver, as an effective therapy for CITRIN deficiency.

1. Introduction

The aspartate-glutamate carriers (AGCs), members of the mitochondrial carrier family, supply aspartate generated in the mitochondrial matrix to the cytosol in exchange for cytosolic glutamate plus a proton [1,2]. Two genes coding for mammalian AGCs have been found, namely *ARALAR/SLC25A12/AGC1* which encodes aralar/AGC1 and *CITRIN/SLC25A13/AGC2* which encodes citrin/AGC2 [3–5], performing essentially the same transport function [2]. The AGCs are components of the malate-aspartate shuttle (MAS) [6]. This shuttle is the main cellular pathway for the transfer of redox equivalents of NADH into mitochondria, which is important in maintaining oxidative glucose consumption and gluconeogenesis from lactate in liver, and allows the mitochondrial synthesis and export of aspartate to the cytosol. This, in turn, is critical for the synthesis of proteins, pyrimidine and purines, i.e., growth related functions [7], and for other cell specific functions as substrate for the urea cycle in hepatocytes or for N-Acetyl-aspartate (NAA) and glutamine synthesis in brain (Fig. 1) [1,8–10].

Aralar and citrin have an overlapping distribution during embryonic development [11]. This distribution changes in the adult in which aralar is found in brain, skeletal muscle, kidney and heart whereas citrin is found predominately in liver, kidney, heart and small intestine [11–13]. Thus, human adult hepatocytes express CITRIN as the main AGC isoform [13] and mutations in *SLC25A13* cause CITRIN deficiency (CD), mainly affecting liver. CD manifests as four different clinical phenotypes: neonatal intrahepatic cholestasis caused by CITRIN deficiency (NICCD) in newborns or infants followed by a silent period in post NICCD patients, after which CD may result in a silent period or manifest as failure to thrive and dyslipidemia caused by CITRIN deficiency (FTTDCD) in some of the post NICCD children, and as citrullinemia type II (CTLN2) in a percentage of adults [14]. So far, no clear link between mutations and clinical outcome has been determined and the reasons why a percentage of adults progresss to CTLN2 is also unknown. CD patients often display, among other symptoms, hypoglycemia, citrullinemia and hyperammonemia, and manifest a striking preference for low sugar and high protein food. The symptoms can be linked directly to the lack of aspartate efflux and MAS activity in absence of functional citrin protein. Indeed, in the liver cytosol, aspartate could be synthesized from oxaloacetate and glutamate by cytosolic aspartate aminotransferase (GOT1; EC 2.6.1.1), but in CD, oxaloacetate formation is limited by the amount of NAD^+. In other words, increases in cytosolic NADH/NAD^+ ratio in CD cause suppression of aspartate formation in the cytosol, and therefore, a block in urea cycle explaining why consumption of excess carbohydrates and reduced compounds such as glycerol or ethanol trigger CD symptoms [10]. Current treatments for CD are low-carbohydrate and high-protein/−fat diets, which are based in the unique food preferences of patients, and sodium pyruvate or medium chain triglycerides supplementation [15]. In the more severe cases, patients can suffer liver failure and the only therapeutic option is liver transplantation [10,16,17].

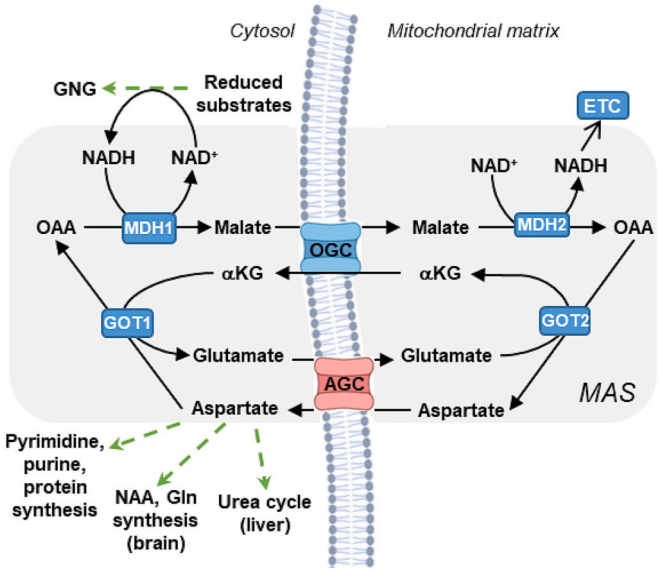

Fig. 1. Function of mitochondrial aspartate-glutamate carriers. Citrin/slc25a13 and aralar/slc25a12 transport cytosolic glutamate (plus H+, not depicted) against mitochondrial aspartate, as part of the malate aspartate shuttle (MAS, shadowed cycle). MAS transfers cytosolic reducing equivalents to mitochondrial matrix for oxidation in the electron transport chain (ETC). Maintenance of cytosolic NAD^+ levels is required for gluconeogenesis (GNG) from reduced substrates in liver. AGCs are also required for net aspartate efflux as substrate for other general purposes such as pyrimidine, purine and protein synthesis, or cell specific pathways as substrate for urea cycle (in the liver) or N-Acetyl-aspartate (NAA) and glutamine (Gln) synthesis in the brain. αKG, alpha-ketoglutarate; OAA, oxaloacetate; MDH1/2, malate dehydrogenase cytosolic/mitochondrial; GOT1/2 aspartate transaminase cysosolic/mitochondrial.

Gene therapy has been shown to represent an attractive and promising alternative for inherited metabolic disorders affecting the liver and other diseases, at least in animal models [18–22]. A major problem faced by gene therapy is the host immune response directed against the viral particle or the transgene product. The latter is of special consideration in the case of non-sense mutations leading to no protein expression, either due to a premature stop codon or instability of the protein. Interestingly, the more prevalent mutations in CD fall in that categories and patients show no protein expression [16,23–25]. It is not known whether the immune system of the patient may react to the recombinant gene product [20,21,26,27]. These facts arise concern of an immune response in the event of gene therapy using the *AGC2* gene.

Aralar shares 78% identity with citrin, has similar transport properties [2], and slightly different calcium regulation properties [28]. Because it is expressed in many cell types, particularly in liver Kupffer cells [11,13], it is unlikely that aralar-based gene therapy would trigger an immune response. Therefore, aralar may be a suitable candidate to substitute citrin in a gene therapy approach, without the risk of activating an immune response.

To explore whether aralar can replace citrin in liver we have addressed the following points: 1. The functional recovery of MAS activity by aralar in *citrin(−/−)* liver by using aralar to replace citrin in mouse *citrin(−/−)* hepatocytes and liver mitochondria. 2. The possible variations in liver redox shuttle systems between mouse and human obtained by absolute quantification proteomics which may influence the use of aralar in gene therapy for CD.

The results obtained indicate that aralar can indeed functionally replace citrin in *citrin(−/−)* mouse liver and that the redox shuttle landscape of human liver makes it likely to benefit from aralar replacement therapy in CD.

2. Methods

2.1. Animal protocols

Animals were housed on a 12-h light/dark cycle, maintained at a temperature of 22 ± 2 °C with a relative humidity of 50% ± 10% and

under pathogen-free conditions. All mice, in the C57BL/6J background, were fed with a standard diet (Tekland Global, ENVIGO) from weaning at 3 weeks of age. All animal experimentation procedures conformed to the European Guidelines for the Care and Use of Laboratory Animals (Directive 86/609) and were approved by the Ethical Committees for Animal Experimentation of the Universidad Autónoma de Madrid and the Comunidad Autónoma de Madrid (PROEX 093/18), Spain. Reporting followed the ARRIVE Guidelines. All efforts were made to minimize the number of animals used and their suffering. All experiments were performed with age-matched animals without gender distinction. Unless otherwise stated, animals were sacrificed by cervical dislocation and liver was fixed in 4% paraformaldehyde (PFA) or used for mitochondrial isolation.

2.2. Transgenic mouse generation

Liver-specific aralar transgenic mice (LAralar Tg) were generated as follows. The full-length mouse *slc25a12/AGC1/aralar* cDNA (pcDNA3.1-Aralar-Flag plasmid supplied by GenScript) was cloned downstream of a liver specific promoter EAlbAAT [29] into pCMV5. To decrease the possibility of silencing [30–32] the β-globin intron was amplified from pTRE2hyg (Clontech) and inserted between the promoter and the aralar cDNA (pCMV5-AlbEnh-βglobin-mAralar, for short pLAralar).

A *Spe*I-*Age*I ~4Kb fragment containing EAlbAAT promoter- intron-aralar-polyadenylation sequences was purified and microinjected into the pronuclei of C57BL/6J *citrin (+/+)*, *citrin (+/−)* or *citrin (−/−)* zygotes [33]. Microinjected zygotes were transferred to pseudopregnant CD1 females. The insertion of transgene in the offspring was analyzed by PCR, using primers derived from β-globin intron (F: 5′- CTAACCATGTTCATCCCTTC-3′) and mouse Aralar (R: 5′-GAGCGGAAATGGAGAGGTGAC-3′) sequences. *Citrin* genotype was determined as described previously [33]. Four independent founders C57BL/6J-EAlbAAT-mAralar were obtained, namely LAralar Tg1-Tg4 lines. Because only transgenic mice on *citrin (+/+)* background were obtained, founders were mated with *citrin (−/−)* mice to produce the desired transgenic mice in *citrin (−/−)* background, LAralar-Tg; *citrin (−/−)*. The colony was maintained by breeding LAralar-Tg;*citrin (−/−)* with *citrin (−/−)* mice or LAralar Tg;*citrin (+/−)* with *citrin (+/−)*.

2.3. Cell cultures

AML12 (ATCC # CRL- 2254) Hep-G2 (ATCC3 #HB-8065) and Huh-7 (Thermo Fisher) were maintained at 37 °C/ 5%CO_2. All lines were grown in the presence of 10% fetal bovine serum (FBS) and antibiotics (penicillin, 100 μg/ml; streptomycin 100 U/ml). AML12 was grown in DMEM:F12 (Thermo Fisher # 11320033) medium supplemented as instructed by supplier; HuH-7 were grown in DMEM (Thermo Fisher #12100061) and Hep-G2 in DMEM supplemented with 2 mM glutamine and 2 mM pyruvate. Primary hepatocytes were isolated from livers of 2–3-month-old wild mice by two-step collagenase perfusion method [34], seeded at 65000 cells/cm^2 in collagen-coated glass coverslips in 24-well plates and maintained in MEM supplemented with 10% FBS, 2 mM glutamine and antibiotics at 37 °C and 5% CO_2 overnight until use.

2.4. Immunocytochemistry

Cell lines were transfected with LTX lipofectamine (Thermo Fisher, A12621) following manufacturer's instructions with pLAralar alone or together with pCMV5-AlbEnh-βglobin-mCitrin-Flag (pLCitrin-Flag) generated similarly to pLAralar from *slc25a13/AGC2/citrin* cDNA ORF Clone (Sino Biological). Fixed cells in 4% PFA were blocked (10% Horse serum, PBS) and probed with polyclonal antibody raised against aralar (1/500; [3]) and either monoclonal antibody against Flag epitope (Sigma, F1804, 1/500) or monoclonal antibody against citrate synthase (Santa Cruz, sc-390693, 1/500) and appropiate secondary antibodies. To visualize nuclei, DAPI (1 μg/ml; Merck) was used. Images were obtained at Axiovert 200 M inverted microscope equipped with a 100×/1.3 Plan-Neofluor objective with appropriate filters.

2.5. Immunohistochemistry

4% paraformaldehyde fixed liver sections were first incubated in antigen retrieval buffer (0.1% SDS, 2 mM EGTA in PBS) for 10 min at 90 °C and treated to quench either endogenous peroxidase (30 min incubation in 3% H_2O_2, 10% methanol, PBS) or autofluorescence (10 min $NaBH_4$ 1 mg/ml in PBS) and blocked in 10% horse serum, 0.5% Triton X-100. Anti-aralar antibody (1/200 in blocking medium, overnight, 25 °C) was detected with biotinylated anti-rabbit antibody (BA2001 Vector, 1/250 in blocking serum), and amplified with Vectastain ABC kit (Vector) before 3′-3`diaminobenzidine (DAB). Alternatively, Alexa 488 Donkey anti-Rabbit (1/500) was used for immunofluorescence detection. Imaging was performed with either Axioskop2 plus microscope (Zeiss) coupled to a color CMOS camera (DMC6200 Leica) and 5×/0.25 -20×/0.15 Plan Neofluar objectives (DAB, HE, PAS, Oil-Red-O) or a Zeiss LSM710 confocal microscope with a 100×/1.40 oil Plan-Apochromat.

2.6. Mitochondrial isolation and MAS activity assay

Mitochondria were isolated from the liver of 6–7 week-old mice of the indicated genotypes, as described previously [28] and were kept on ice in MSK medium (in mM: 75 mannitol, 25 sucrose, 5 potassium phosphate, 20 Tris-HCl, 0.5 EDTA, 100 KCl, and 0.1% bovine serum albumin, pH 7.4) or stored at −80 °*C*. MAS activity was reconstituted essentially as previously described [28,35]. Briefly, 0.1–0.15 mg of liver mitochondria were resuspended in 2 ml of MSK and the shuttle was reconstituted in the presence of 4 U/ml aspartate aminotransferase (GOT, Sigma G-2751), 6 U/ml malate dehydrogenase (MDH, Sigma M1567), 66 μM NADH, 5 mM aspartate, 5 mM malate, 0.5 mM ADP and 200 nM Ruthenium Red (RR). To remove contaminant α-ketoglutarate from GOT, the enzyme was dialyzed in 3 M $(NH_4)_2SO_4$ + 1 mM pyridoxal phosphate for 48 h at 4 °C with shaking in a ratio of 1:100 (vol enzyme: vol solution). 10 μM free Calcium (calibrated by Fura-2 and Calcium Green as described in [28]) was present when indicated. Activity determined as the NADH decay rate after triggering the reaction with 10 mM glutamate addition, corrected for glutamate-independent NADH decay and protein content (Bradford method) in the assay. Mitochondria preparations from paired LAralar Tg and non-transgenic mice of *citrin (−/−)* background from age-matched pairs were generated and analyzed on the same day.

2.7. Western blot

Mitochondrial proteins were separated by SDS-PAGE (8%) electrophoresis, transferred onto Nitrocellulose membranes and dyed with Ponceau Red, to assess for protein load. The membranes were blocked (5% Skim Milk, Nestlé, 0.5%Tween20 in TBS) and probed with antibodies against aralar (1/5000), citrin (1/3000; [11]) and either β-ATPase (1/5000, [36]) or citrate synthase (1/4000). After extensive washing (2% milk, 0.1% Tween20 in TBS), membranes were incubated with appropriate secondary antibodies conjugated with horseradish peroxidase and the signal was detected by chemiluminescence (ECL, PerkinElmer), as described earlier [11]. Analysis of resulting bands was performed with ImageJ software.

2.8. Measurement of NADH/NAD^+ and ATP/ADP ratios

Single-cell measurements of cytosolic NADH/NAD^+ or ATP/ADP ratios were obtained in transfected hepatocytes with plasmids coding for nuclear ratiometric Peredox-mCherry [37,38] or for cytosolic ratiometric Perceval-HR [39] respectively and used 24–36 h later. Transfection was performed using Polyethilenimine (PEI 25K™, Polysciences, Cat No. 23966), at a 1:3 (DNA:PEI, w:w) ratio. For exogenous expression

of aralar, hepatocytes were co-transfected with pcDNA3.1-Aralar-Flag (GeneScript). Co-transfection was confirmed by immunocytochemistry in 4% PFA fixed cells at the end of assay. Experiments were performed at 37 °C on an Axiovert 200 M inverted microscope equipped with a 40 × /1.3 Plan-Neofluar objective and an ORSA Flash 4.0 camera (Hamamatsu) illuminated with a CoolLED PE-300 light source. Coverslips were preincubated in imaging medium (IM, in mM:100 HEPES, 121 NaCl, 4.7 KCl, 1.2 KH_2PO_4, 1.2 $MgSO_4$, 1.2 $CaCl_2$) supplemented with 2.5-5 mM glucose for 15 min before recording.

For Peredox (NADH/NAD^+ ratio) time lapse imaging, cells were excited alternatively at 381–404 nm (cpGFP-TSapphire) and 543–558 nm (mCherry); emitted fluorescence was collected at 505–530 nm and 580–611 nm respectively. Peredox emission ratio was TSapphire/mCherry (F405/F555) reflecting cytosolic NADH/NAD^+ ratio. For Perceval-HR (ATP/ADP ratio) imaging, cells were excited alternatively at 423–448 nm (Venus) and 472–494 nm (GFP); emitted fluorescence was collected at 505–530 nm (GFP), with emission ratio GFP/Venus reflecting ATP/ADP ratio. 20 images were recorded for basal detection of ratios before addition of either 25 mM pyruvate or 10 mM lactate (Peredox) or 5 μM oligomycin (Perceval-HR). Images were adquired every 5 s. Single-cell fluorescence recordings were analyzed using ImageJ and Excel software.

2.9. Human sample collection

Human liver samples used in this study were obtained from anonymized adult individuals (42 to 56 years old) undergoing bariatric surgery and laparoscopic liver biopsy. Part of the specimen was included in formaldehyde for histological analysis and the other was stored at −80 °C. The study was approved by the Ethics Committee of the 'Hospital Universitario 12 de Octubre' (Madrid, Spain) (protocol code: 19/210, Date of approval 28/05/2019), which was performed in accordance with the Declaration of Helsinki for Human Research. For isolation of mitochondria from frozen samples, 150–200 mg of frozen tissue were quickly homogenized in IM (mM: 250 sucrose, 25 HEPES, 10 KCl, 1 EDTA, 1 EGTA, 1.5 $MgCl_2$, 1 dithiothreitol, 1 phenylmethylsulfonylfluoride, 1 iodoacetamide). After homogenization, mitochondrial fractions were obtained by differential centrifugation as described previously. For comparison, mouse liver mitochondria were similarly prepared from frozen tissue.

2.10. Mitochondrial proteomics by data-independent scanning mass spectrometry

Blue native gel electrophoresis (BNGE) gels were excised in 26 slices taking as reference some discrete Coomassie-stained bands from the same sample: slice 6 corresponds to a band that mainly contains supercomplex I + III_2, slice 10 to CV (ATP synthase), slice 12 to free supercomplex III_2, and slice 15 to free CIV. All slices were in-gel digested with trypsin. The resulting tryptic peptide mixtures were subjected to nano-liquid chromatography coupled to tandem mass spectrometry using a data-independent scanning (DiS) method as described previously [40]. In brief, peptides were injected onto a C-18 reversed phase (RP) nano-column (75 μm I.D. and 50 cm, Acclaim PepMap, Thermo Fisher, San José, CA, USA) and analyzed in a continuous acetonitrile gradient consisting of 8–31% B for 130 min, 50–90% B for 1 min (B = 0.5% formic acid in acetonitrile). Peptides were eluted from the RP nano-column at a flow rate of ~200 nl min^{-1} to an emitter nanospray needle for real-time ionization and peptide fragmentation in either a Q-Exactive or a Q-Exactive HF mass spectrometer (Thermo Fisher). Each sample was analyzed in two chromatographic runs covering different mass ranges (from 400 to 750 Da, and from 750 to 1,100 Da, respectively). The DiS cycle consisted of 175 sequential HCD MS/MS fragmentation events with 2-Da windows that covered the whole 350 Da range. HCD fragmentation was performed at a resolution of 17,500 and a maximum injection time of 80 ms with the AGC set to a target of 3×10^5 ions. The whole cycle lasted 30 s or less depending on ion intensity during chromatography. The narrow windows used for fragmentation allowed peptide identification using conventional shotgun searching algorithms. This was done using Sequest running under Proteome Discoverer 1.4 (Thermo Fisher Scientific), allowing two missed cleavages, and using 2 Da and 20 p.p.m. precursor and fragment mass tolerances, respectively. Met oxidation and Cys carbamydomethylation were selected as dynamic or static modifications, respectively. 1% FDR was used as a criterion for peptide identification; this parameter was estimated using a separate inverted database.

2.11. Peptide synthesis for Parallel Reaction Monitoring (PRM) assays

The selection of the peptides used in the PRM assays was carried out following the usual criteria in the design of targeted proteomics experiments and using previous information obtained through shotgun proteomics assays. Synthetic peptides were used to validate PRM methods, to confirm the sequence identity, and for absolute quantitation. Synthesis, both for light and heavy versions of the peptides, was carried out in-house using standard Fmoc chemistry in an Intavis Multiple peptide synthesizer (INTAVIS, Cologne, Germany). After HPLC purification (>90%), synthetic peptides were quantified using amino acid analysis.

2.12. Parallel Reaction Monitoring (PRM) analysis

15 micrograms of each of the samples were digested with trypsin on STRAP columns (PROTIFI, Farmingdale, NY), according to the protocol described by the manufacturer. Tryptic peptides were dried in a speed-vacuum system and resuspended at 200 ng/μl, according to QUBIT quantification (Thermofisher Scientific). 5 μL of each sample (equivalent to 1 μg) were loaded online on a C18 PepMap 300 μm I.D. 0.3 × 5 mm trapping column (5 μm, 100 Å, Thermo Scientific) and analyzed by LC-ESI MSMS using a Thermo Ultimate 3000 RSLC nanoUPLC coupled to a Thermo Orbitrap Exploris OE240 mass spectrometer. Peptides were separated on a 15 cm, 75 μm ID column, with a flow rate of 300 nl/min and a 60 min long gradient. The liquid chromatographic system was coupled via a nanospray source to the mass spectrometer. The mass-spec method used worked in PRM mode (parallel reaction monitoring) monitoring the six selected peptides (3 per protein) both in light and heavy format. Selection and extraction of each of the transition areas (see Supplementary Table 1), was carried out with the Skyline v21.2 software [41]. Heavy peptides were PRM-analyzed at different amounts (ranging from 63 attomol to 1000 fentomol) and used to raise a linear regression model that was used to estimate the actual amount of the internal (light) peptides in the samples.

2.13. Statistical analysis

The results are expressed as the mean ± standard error of the mean (SEM) the sample size for each experiment is indicated in the figure legends. As general rule comparisons were planned between age-matched pairs of siblings LAralar Tg;*citrin (−/−)* and *citrin (−/−)*. Gender was not taken into consideration. All statistical analyses were performed using GraphPad Prism v.7.01 for Windows.

3. Results

3.1. Exogenous aralar reverts the increase in cytosolic NADH/NAD^+ ratio in citrin KO hepatocytes

To investigate whether increasing aralar levels may constitute a suitable replacement for missing citrin activity in CD, we first performed an in vitro approach using primary hepatocytes from *citrin(−/−)* mice. *Citrin (−/−)* mice have decreased MAS activity in liver mitochondria but otherwise a very mild phenotype that does not recapitulate CD [42]. MAS deficiency in CD is predicted to impair the regeneration of NAD^+,

when using reduced substrates such as glucose or lactate Therefore, we focused on the cytosolic ratios of NADH/NAD$^+$ and ATP/ADP in hepatocytes using glucose using the corresponding sensor for single cell analysis in primary hepatocytes.

The NADH/NAD$^+$ ratio was studied in hepatocytes transfected with Peredox, a genetically encoded fluorescent sensor that enables specific measurement of free cytosolic NADH/NAD$^+$ ratio in intact cells [37,38]. In Peredox, the NADH/NAD$^+$ sensing part of the probe (based on GFP-TSapphire protein) is bound to a C-terminal RFP mCherry to normalize for the green fluorescence. Therefore, variations in the basal Peredox fluorescence ratio (T-Sapphire normalized for mCherry) report variations in NADH/NAD$^+$. We have employed nuclear targeted Peredox as we observed that its cytosolic version led to aggregates as previously reported [38], which were absent with the nuclear version, and there is no difference in the NADH/NAD$^+$ ratio between cytosol and nucleus [38]. Fig. 2A shows the pattern of nuclear Peredox in hepatocytes. We have verified that cells co-transfected with Peredox and pcDNA3.1-Aralar-Flag expressed both proteins, as shown in Fig. 2A.

Experiments were run at 5 mM glucose, a concentration similar to that present in fasted animals, when citrin is expected to play a major role in gluconeogenesis from certain substrates. As expected, the basal NADH/NAD$^+$ ratio in hepatocytes from *citrin (−/−)* mice was higher than that of *citrin (+/+)* mice (Fig. 2B), consistent with a failure in MAS and the transfer of reducing equivalents to mitochondria. A similar increase in basal cytosolic NADH/NAD$^+$ ratio was observed in epithelial cells in which citrin was silenced [43]. In the presence of exogenous aralar, basal NADH/NAD$^+$ ratio dropped to values similar to those of *citrin (+/+)* hepatocytes (Fig. 2B). Addition of pyruvate used as control induced a decrease in the NADH/NAD$^+$, with a similar rate of decrease in all preparations, at least in the time frame of our protocol (Fig. 2C).

We also studied basal NADH/NAD$^+$ ratio in hepatocytes incubated with at a lower glucose concentration, 2.5 mM. The difference in basal Peredox ratio between *citrin (+/+)*, *citrin (−/−)* and *citrin (−/−)* hepatocytes expressing exogenous aralar was also clearly observed at 2.5 mM glucose (Fig. 2D). Of note, *citrin (+/+)* hepatocytes responded faster and to a larger extent to lactate addition than *citrin (−/−)* hepatocytes (Fig. 2E). This is consistent with a higher basal NADH/NAD$^+$ ratio in *citrin (−/−)* hepatocytes, closer to the maximum. Expression of exogenous aralar in *citrin (−/−)* hepatocytes lowered the NADH/NAD$^+$ and modified the dynamic response to lactate, to values similar to *citrin (+/+)* (Fig. 2E).

Next we evaluated whether citrin deficiency affects the cytosolic ATP and ADP levels in hepatocytes from *citrin (−/−)* mice using the ratiometric probe Perceval-HR to detect cytosolic ATP/ADP ratio [39]. We observed no differences in the basal ATP/ADP ratio between *citrin (+/+)* and *citrin (−/−)* hepatocytes, and the expression of exogenous aralar was without effect (Fig. 2F). Inhibition of oxidative phosphorylation (OXPHOS) by oligomycin (5 μM) elicits an immediate decrease in the ATP/ADP ratio which has been studied in neurons lacking aralar and shown to be different than that of control neurons [44]. However, the drop in cytosolic ATP/ADP ratio was the same in *citrin (+/+)* or *(−/−)* hepatocytes (results not shown) supporting the maintenance of this ratio

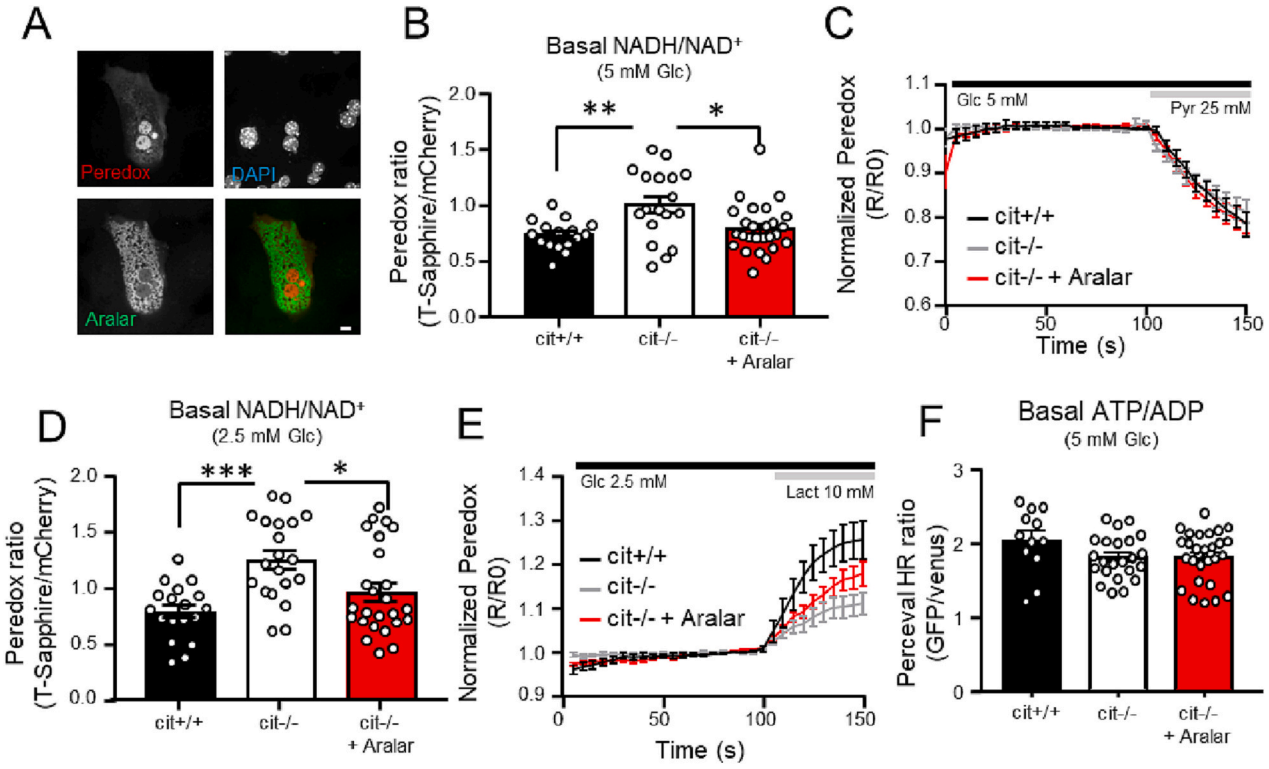

Fig. 2. Exogenous Aralar reverts the increase in cytosolic NADH/NAD$^+$ ratio in citrin deficient hepatocytes. A. Representative images from *citrin (−/−)* hepatocytes co-transfected with nuclear-targeted Peredox and pcDNA3.1-Aralar-Flag (red and green signals, respectively, in merged panel). Nuclei are stained with DAPI. Scale bar is 10 μm. B. Basal cytosolic NADH/NAD$^+$ determined as T-Sapphire to mCherry fluorescence ratio (Peredox ratio) from Peredox-transfected hepatocytes of the indicated genotypes in the presence of 5 mM glucose. When indicated (+Aralar), co-transfection with Aralar-Flag was carried out. C. Change in NADH/NAD$^+$ ratio upon addition of 25 mM pyruvate. Data are mean ± SEM of 16 *citrin (+/+)*, 18 *citrin (−/−)* and 26 *citrin (−/−)* + pAralar-Flag Peredox-positive cells from three independent hepatocyte preparations. D. Basal cytosolic NADH/NAD$^+$ determined as in B from hepatocytes in the presence of 2.5 mM glucose. When indicated (+ Aralar), co-transfection was performed as in B. E. Change in NADH/NAD$^+$ ratio upon addition of 10 mM lactate. Data are mean ± SEM of 18 *citrin (+/+)*, 20 *citrin (−/−)* and 25 *citrin (−/−)* + pAralar-Flag ells from three independent hepatocyte cultures. F. Basal ATP to ADP ratio as determined by GFP to Venus fluorescence ratio by the ratiometric probe Perceval-HR. Data are mean ± SEM of indicated 12 *citrin (+/+)*, 23 *citrin (−/−)* or 29 *citrin (−/−)* + pAralar-Flag Perceval-HR-positive cells from three independent hepatocyte preparations. Statistical significance (***$p < 0.0005$; ** $p < 0.005$, * $p < 0.05$) was determined by one-way ANOVA followed by Bonferroni post hoc test.

in hepatocytes from citrin deficient mice.

3.2. Exgoneous aralar partially recovers malate aspartate shuttle activity in liver mitochondria from citrin deficient mice

To further investigate whether increasing the levels of aralar could replace citrin activity in vivo in *citrin(−/−)* mice, we generated a transgenic mouse model expressing aralar under the transcriptional control of a liver specific promoter. To drive the expression of the transgene, we chose the chimeric promoter formed by the distal mouse Albumin Enhancer and the minimal alpha-1- antitrypsin promoter (EAlbAAT), which has been shown to produce high levels of transgenic protein in hepatic cells lines and in mouse liver [29]. We included the β-globin second intron, as its inclusion improves transgene expression [30–32] (Fig. 3A).

The functionality of LAralar transgene was tested by transient transfection in hepatic cell lines of mouse and human origin. Transfected cells showed expression of aralar protein, which colocalized with citrate synthase, a mitochondrial matrix enzyme (Fig. 3B). When expression of citrin, under the same promoter, was analyzed together with aralar, both proteins were found to colocalize (Fig. 3C). These results validated the correct expression and targeting of the exogenous protein. Therefore the expression cassette was digested from the plasmid, purified and microinjected in zygotes of *citrin (+/+)*, *citrin (+/−)* or *citrin (−/−)* genotypes, all in C57BL/6J background. Out of 815 zygotes injected and implanted in pseudopregnant foster dams, 47 were born and 24 survived for genotyping. Four founders (F0), LAralar Tg1-Tg4 (all obtained in *citrin (+/+)* background) were shown to have acquired the transgene and to transmit it to their offspring (F1) as detected by specific PCR (Fig. 3D).

In LAralar Tg-1 mice, transgene mRNA was not detected and consistently no increase in protein was found (not shown). Aralar levels were increased by 2.25 fold in LAralar Tg2 mice and 1.7 fold in LAralar Tg 4 mice lines, as compared with control mice (Fig. 3E, F). However, LAralar Tg-3 only showed a marginal increase in aralar protein levels. As LAralar Tg-2 was the transgenic line with the highest aralar levels we chose it for further studies.

We have also examined the presence of exogenous aralar in the liver of LAralar Tg mice by 3,3-diaminobenzidine (DAB) immunohistochemical-staining (brown clusters) or immunofluorescence using anti-aralar antibody. As shown in Fig. 3G, endogenous aralar is almost undetectable in liver tissue from *citrin (+/+)* mice, whereas in the transgenic line scattered groups of aralar-positive cells were found showing an intense mitochondrial-like staining (Fig. 3H). The number of positive cells and their distribution varies between sections and animals. This uneven distribution is not an uncommon characteristic in other models where foreign genes are expressed in liver [45–47]. In this particular case, one of the elements of the transgenic vector, alpha-1-antitrypsin promoter, has been reported to be silenced in vivo [48]. However the exact mechanism has not been explored.

To test the function of exogenous aralar in liver of LAralar Tg;*citrin (+/−)* or LAralar Tg;*citrin (−/−)* mice, we examined its effect in MAS activity reconstituted in liver mitochondria. MAS activity dropped by ~50% in mitochondria from *citrin (−/−)* mice (13.9 ± 3.2 nmol NADH min^{-1} x mg $prot^{-1}$) as compared with *citrin (+/+)* mice (33 ± 4.3 nmol NADH min^{-1} x mg $prot^{-1}$). The effect of LAralar Tg in the liver of *citrin (−/−)* mice was found to be a small but consistent increase in MAS activity of ~ 4–6 nmol NADH min^{-1} x mg $prot^{-1}$ (Fig. 3I). A similar increase was also observed when *citrin(+/−)* mice were used (not shown). MAS activity is regulated by extramitochondrial calcium most likely by binding to Ca^{2+}-binding EF-hand motifs present in the amino terminal domain of the AGCs [1,28]. Ca^{2+} addition caused an increase in residual MAS activity of *citrin (−/−)* mitochondria (1.64 fold) which was also found in the presence of the transgene (1.46 fold). (Fig. 3I). The relatively small effect of transgenic aralar in the MAS reconstitution assay may be explained by its patchy distribution, whereby only a small percentage of liver cells have increased aralar levels. In any event, this increase, albeit small, shows that exogenous aralar is functional in liver, ~~in~~ the context of shuttle activity without affecting calcium sensitivity.

3.3. Aralar is present in the mouse liver but only at very low levels in human liver

The experiments shown so far indicate that the presence of exogenous aralar in mouse liver and in mouse hepatocytes may restore citrin function. However, we found an unexpected high level of residual MAS activity in the absence of citrin. Because we have detected by western blot the presence of endogenous aralar in our mouse model, the residual activity could be explained by endogenous aralar (see Fig. 3E,F). The presence of aralar in mouse liver contrasts with conclusions from previous studies in rat [11] and human liver [13], but aligns with proteomics studies in liver mitochondria pointing to substantial expression of aralar in the mouse liver ([49], supplemental Fig. 1), whereas proteomic assays in human liver hardly detect aralar [50]. Therefore, we have studied citrin and aralar levels in three samples from human liver biopsies and determined the citrin/aralar ratio with the use of Absolute Quantification methods, and compared them to the values in mouse mitochondria.

Isolation of mitochondria was required to be able to detect ARALAR in human liver, as it was not detected in whole extracts (results not shown). As we started from frozen liver samples, we first verified whether citrin and aralar are maintained in mitochondria extracted from frozen tissue. Mitochondria extracted from frozen mouse liver lose some matrix proteins (as citrate synthase, Supplemental Fig. 2) while maintaining a high protein content and citrin/aralar ratio. Therefore, the same mitochondria isolation procedure was applied to human liver samples. Whole protein extracts from liver mitochondria (500 ng) were trypsin digested and analyzed with a liquid chromatographer Thermo Ultimate 3000 (gradient length 120 min) coupled to a Thermo Orbitrap Exploris OE240 Mass Spectrometer, working in DDA (Data Dependent Acquisition) mode. MS1 and MS2 spectra were used to launch a database search, using Proteome Discoverer v2.4 and four different search engines (Mascot, Amanda, MSFragger and Sequest). Additional searches were performed using Peaks v7.5. >3000 protein groups were identified, which included CITRIN, but ARALAR was not among them.

In order to increase the depth of the proteomic analysis, whole mitochondrial protein extracts were separated by SDS-PAGE gels and the area around 70, where both citrin and aralar migrate, was cut in five slices (Supplemental Fig. 2). Each gel slice was in-gel trypsin digested and the resulting tryptic peptides analyzed by LC-MS as indicated above (using a shorter gradient). A variable number of proteins, between 350 and 750 proteins, were identified in each gel slice, confirming that this approach increased significantly the coverage of the liver proteome. Citrin was identified in all 5 slices, with slice #3 being particularly rich in citrin peptides. Aralar was identified as well in slice #3 but the short number of peptides identified (eight) suggested that it was much less abundant than citrin. We selected three unique (proteotypic) peptides (Fig. 4A, B) for each AGC in order to produce AQUA (Absolute QUAntification) peptides that would be used in PRM (Parallel Reaction Monitoring) targeted proteomics experiments. These selected peptides were common for human and mouse AGCs so they could be used to quantify the citrin to aralar ratio in both species. AQUA peptides were synthesized in heavy format, HPLC-purified, quantified, and tested for linear behavior in tryptic extracts (Fig. 4C—F). We found all six peptides suitable for absolute quantification in a targeted analysis. We have used them to quantify aralar and citrin in mitochondrial fractions obtained from three human and two mouse liver samples (Fig. 4G).

For human samples, the values obtained for endogenous aralar peptides are in the lower range of the calibration curve represented using different concentrations of synthetic heavy peptides. This affects quantification but reflects the low abundance of aralar in human liver. The mean of all values gives a CITRIN to ARALAR ratio of around 397 in

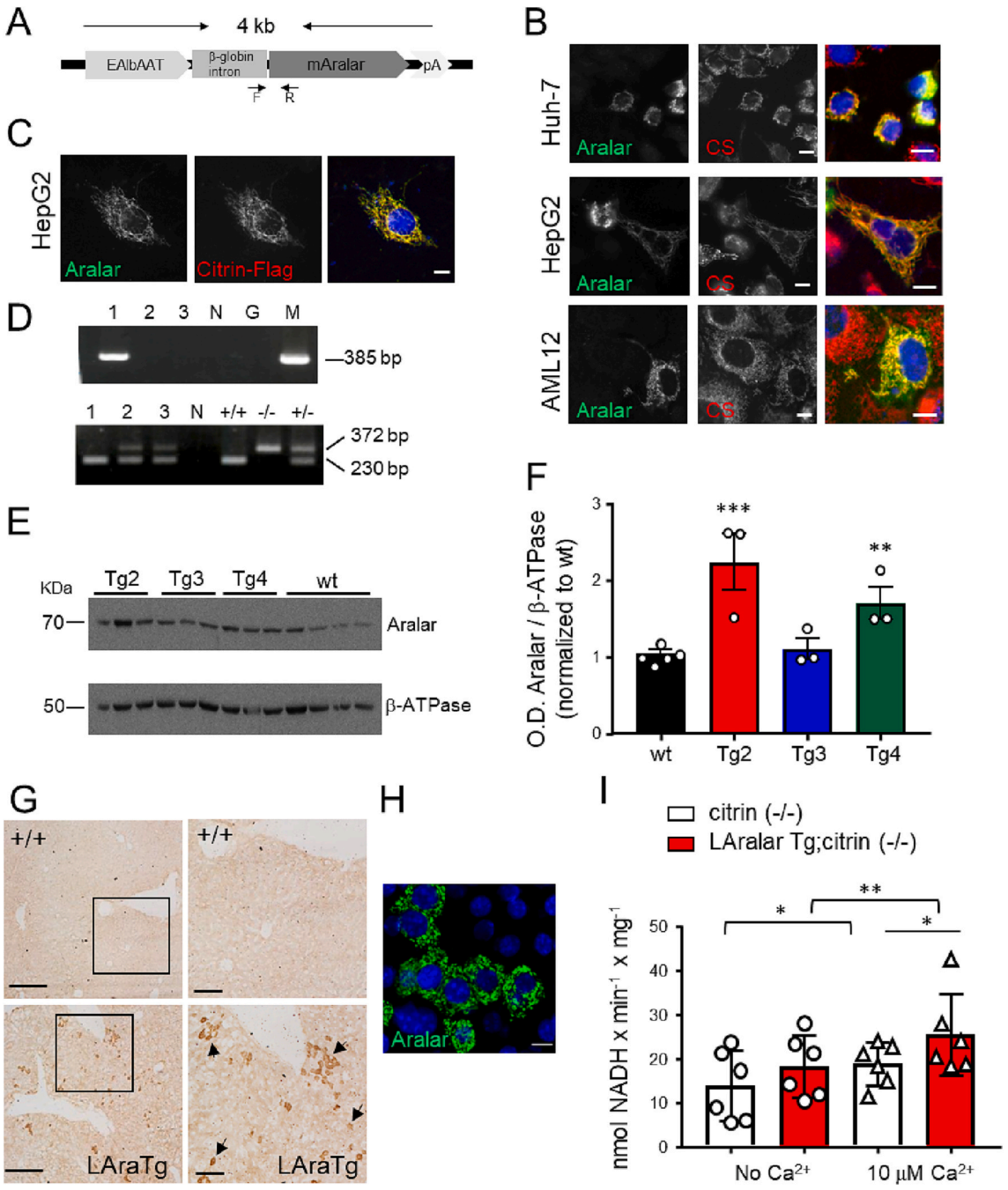

Fig. 3. Generation of a transgenic mouse expressing Aralar in liver. A. Schematic diagram of the Liver-Aralar transgene (LAralar Tg) construct. Relative positions of forward (F) and reverse (R) primers used for PCR genotyping are showed. B. Immunofluorescence assay with anti-aralar and anti-citrate synthase (CS, as mitochondrial marker) antibodies of human (Huh7 or Hep-G2) and murine (AML-12) hepatic cell lines transfected with pLAralar. The enlarged merged images show the complete colocalization of aralar (green) and mitochondrial CS (red) signals. Nuclei are stained with DAPI (blue). Scale bar 10 μm. C. Immunofluorescence assay of Hep-G2 cells co-transfected with pLAralar and pLCitrinFlag. Merged image shows the colocalization of anti-aralar (green) and anti-Flag (red) signals. Nuclei are stained as in C. Scale bar 10 μm. D. Upper panel, genotyping of a litter of 3 mice to detect transgene insertion by PCR amplification. Lower panel, genotyping for citrin of the same litter. Controls: H_2O (N), wild type genomic DNA (G), pLAralar plasmid (P), and *citrin* (+/+), (+/−) or (−/−) genomic DNA were used. E, F. Immunoblot analysis (E) and quantification (F) of aralar levels in liver samples from the indicated LAralar Tg transgenic mouse lines. Quantification relative to the mitochondrial loading control (β-ATPase) and to aralar levels in wt mice is shown Data are represented as the mean +/− SEM of 5 (wt), 3 (Tg2–4) mice. ** $p < 0.01$; *** $p < 0.005$, ANOVA and followed by Bonferroni post hoc test. G,H Immunohistochemistry of aralar in PFA-fixed liver sections. Representatives 3,3′-Diaminobenzidine (DAB) staining patterns (G) of aralar in liver sections from control (upper panels) and LAralar Tg (lower panels). Aralar-positive cells (brown) appear exclusively in LAralar Tg sections but are distributed in scattered clusters (arrows). Right panels show enlarged insets in left panels. Scale bar is 300 (leftpanel) and 100 μm (right panel). H. Representative confocal image of immunofluorescence of aralar (green) in liver section from LAralar Tg mice confirming its mitochondrial distribution. Nuclei are stained with Topro-3. Scale bar is 10 μm. I. MAS activity was determined *citrin (−/−)* liver mitochondria without or with transgene expression *(LAralar Tg;citrin (−/−))*. Experiments were performed in non-stimulated (No Ca^{2+}) and stimulated (10 μM free Ca^{2+}) conditions. Data represent mean ± SEM of six paired mitochondrial preparations assayed at least in triplicate. ** $p < 0.005$, * $p < 0.05$ Two-way ANOVA repeated measures followed by Bonferroni post hoc test.

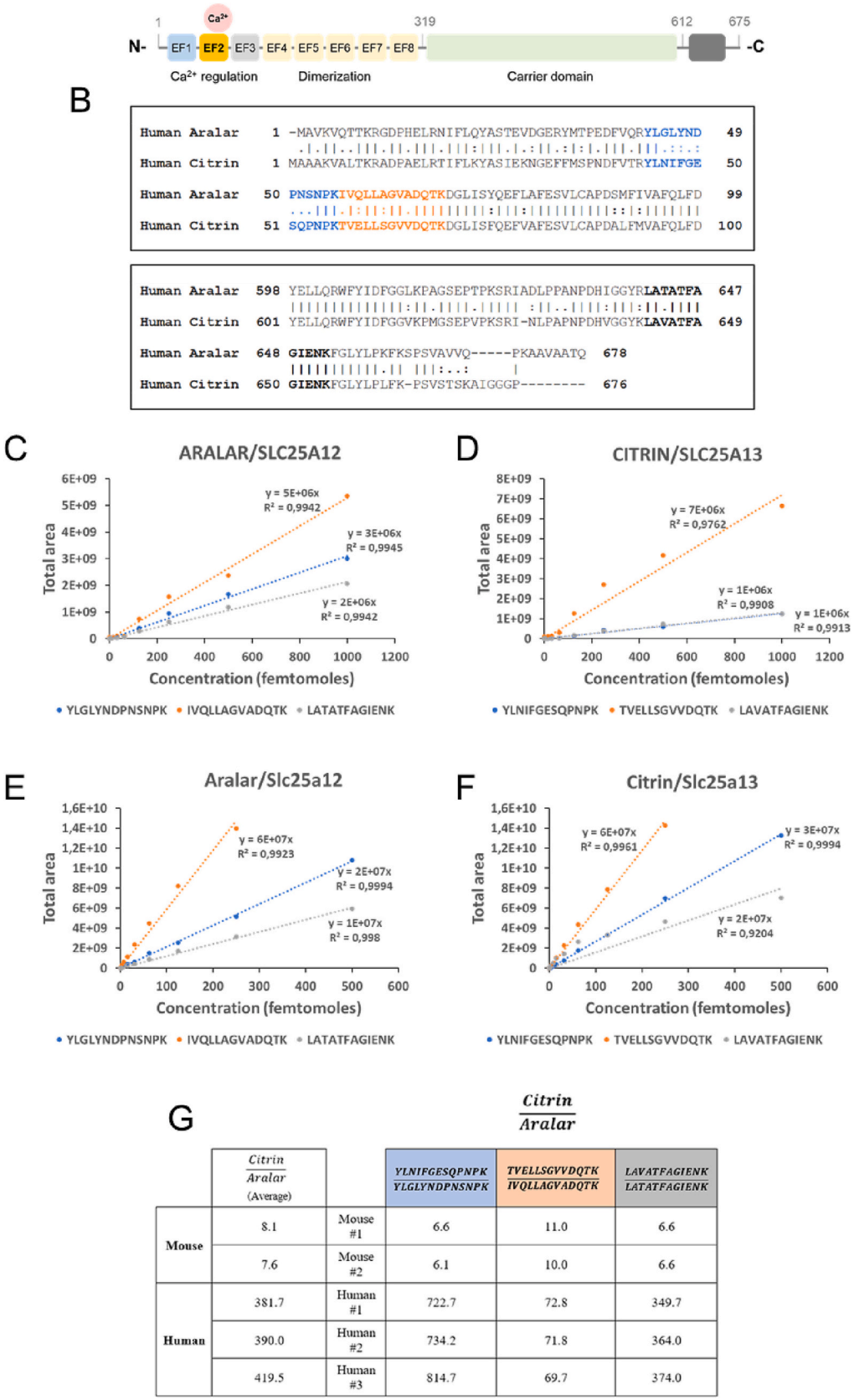

Fig. 4. Absolute quantification of aralar and citrin in human and mouse liver mitochondria. A. Scheme of AGCs structure, showing the N-terminal domain harboring the 8 EF hands, the carrier domain and the C-terminal domain. B. Partial sequence alignments of human ARALAR and CITRIN, showing the three peptides selected for the AQUA quantification in blue, orange and black (colors correlate with scheme of panel A). The peptides selected are respectively conserved in mouse aralar and citrin so they can also be used for the quantification of mouse samples. C—F. Calibration curves generated with AQUA peptides for human ARALAR (C) and CITRIN (D), as well as for mouse aralar (E) and citrin (F). Linear regressions are shown in dotted lines. G. AQUA quantification of citrin/aralar in three human and two mouse liver mitochondrial fractions with each pair of peptides.

G

	$\frac{Citrin}{Aralar}$ (Average)		YLNIFGESQPNPK / YLGLYNDPNSNPK	TVELLSGVVDQTK / IVQLLAGVADQTK	LAVATFAGIENK / LATATFAGIENK
Mouse	8.1	Mouse #1	6.6	11.0	6.6
	7.6	Mouse #2	6.1	10.0	6.6
Human	381.7	Human #1	722.7	72.8	349.7
	390.0	Human #2	734.2	71.8	364.0
	419.5	Human #3	814.7	69.7	374.0

human liver (analysis with 3 peptides) or 560 (analysis with 2 peptides).

For mouse samples, the signal corresponding to the endogenous (light) peptides from both aralar and citrin was high and, therefore, it did not affect to the accuracy of the quantification. As for human samples, two of the peptides give a similar ratio, somewhat different than that obtained for the pair of peptides IVQLLAGVADQTK/TVELLSGVVDQTK. This renders a citrin to aralar ratio in mouse liver of around 7.8 (analysis with 3 peptides) or 6.4 (analysis with 2 peptides), very similar to that obtained (4.5) in the mouse proteomic study shown in Supplementary Fig. 1 with data from high molecular weight complexes rather than whole mitochondria.

The results shown here reflect the low abundance of ARALAR in human liver as compared to mouse liver. Hence, the mild in vivo phenotype in the citrin knock out mouse [42] may be explained by the presence of endogenous aralar in mouse as compared with human liver, among other species differences.

4. Discussion

4.1. Exogenous aralar to replace citrin

The *citrin (−/−)* mouse does not does not recapitulate traits observed in CD patients such as hypoglycemia, hyperammonemia, or citrullinemia among others [42], and it is thus an inappropriate CD model for in vivo experiments. However, *citrin(−/−)* mouse does show a drop in MAS activity in liver and an increase in lactate/pyruvate ratio in liver perfusate [42], which can be used as readouts for the efficacy of citrin replacement with exogenous aralar. This study shows that exogenous aralar can replace citrin functions in mouse liver mitochondria (MAS activity) and hepatocytes (NADH/NAD^+ ratio), at least to some degree. We report a normalization of NADH/NAD^+ ratio by exogenous aralar in acutely isolated hepatocytes from *citrin (−/−)* mice, and an increase in MAS activity in liver mitochondria from LAralar Tg:+*citrin(−/−)* mice compared to that of *citrin (−/−)* mice.

In our study, the increase in aralar levels caused by transgene expression in liver is ~ 2.25 fold and represents an increase in MAS activity of ~ 4–6 nmol NADH min^{-1} x mg $prot^{-1}$, or around ~ 15% of liver MAS activity (~33 nmol NADH min^{-1} x mg $prot^{-1}$). Assuming that exogenous and endogenous aralar have the same activity as MAS components, endogenous aralar would contribute to mouse liver MAS in about ~4 nmol NADH min^{-1} x mg $prot^{-1}$, or ~ 12% of MAS activity in liver. Considering the 7.8:1 citrin to aralar molar ratio in mouse liver, these numbers would support similar activity of citrin and aralar as aspartate/glutamate exchangers, which together with the maintenance of Ca^{2+} sensitivity, would support the use of aralar as surrogate for citrin in gene therapy.

Cao et al. [51] explored the possibility of using a hCitrin-mRNA in lipid nanoparticles (LNP) based therapy to treat CD in the double KO CD model (citrin and glycerolP-DH/GPD2 KO) [52], in which the lack of the second redox shuttle gives rise to an improved CD model. LNP are taken up by the liver through the ubiquitous low-density lipoprotein receptor [53], which would allow a homogeneous level of hCitrin protein in all hepatocytes. While glycemia or MAS activity were not reported in the study, aversion to sucrose was found in these double KO mice [51,52], which was reverted by hCitrin-mRNA-LNP delivery. The hCitrin protein levels attained in the liver of the double KO mouse were calculated to be ~ 2–5% of endogenous citrin [51]. This suggests that a modest increase in AGC levels (and MAS activity) as that obtained with the use of liver specific transgenic aralar may be able to revert the effects of CD, especially under conditions in which aralar levels are increased in a mild but uniform way throughout the liver. In addition, delivery of aralar-mRNA using LNP may be successful in gene therapy for CD. In this regard, the delivery of AGC-mRNA LNP or other means of increasing aralar or citrin levels in liver needs to be adjusted so as to avoid high levels of either of the two which have been associated with different cancer types in liver and other tissues [54–57]. However, the citrin KO mouse model does not present the relevant clinical symptoms or the acute life-threatening hyperammonemia or liver damage in CTLN2, and any aralar-based therapy would not provide useful information when used on this mouse. Therefore, further studies would require a better CD model in which the metabolic derangement of CD could be reproduced, such as the double KO (global citrin and GPD2 KO) or double AGC KO in liver (citrin KO and liver specific Aralar KO). The use of these and other mouse CD models will be required to reproduce the clinical CD symptoms in the mouse and to explore the possible reversal of each of them with the use of exogenous aralar or citrin.

4.2. Human redox shuttles in liver

A most relevant finding in this study is the huge difference between aralar levels in human and mouse liver, with a citrin to aralar molar ratio of about 400 in human and about 8 in mouse. This difference agrees with data from label-free proteomic studies as shown in Table 1 which also show that mitochondrial glycerol-3-phosphate dehydrogenase (GPD2), the mitochondrial component of the glycerol phosphate shutttle (GPS) is also very much enriched in mouse with respect to human liver (Table 1).

Human CD emerges as a condition in which the liver lacks the main redox shuttles, unlike the mouse, in which an active GPS and aralar-MAS still maintain redox functions. This explains the extremely mild phenotype of the *citrin (−/−)* mouse, and the appearance of some of the traits of human CD in the double knock out mouse, lacking both citrin and GPD2 [52], clearly indicating that the loss of redox shuttles is a major defect explaining human CD. Indeed, hyperammonemia in CD patients and in the mouse citrin and GPD2 double knock out is observed under fed rather fasted conditions [52], suggesting that the high carbohydrate meal which entails redox shuttle activity is associated with impaired disposal of ammonia.

There is increasing evidence that in most cell types the MAS and GPS can replace one another and that the total capacity of the redox shuttles limits OXPHOS from glucose so that only when these shuttles become saturated glucose use is diverted into lactate production rather than OXPHOS [58–60]. In other words, redox shuttles limit the fate of glucose in most cells and in the case of the liver, they would also limit the use of lactate as a substrate for gluconeogenesis. Therefore, increasing the liver redox shuttle capacity in CD emerges as a promising strategy towards a cure of the condition.

The finding that aralar can partially replace citrin as MAS component in mouse liver is an important step towards its possible use in gene therapy for CD. Aralar therapy is expected to increase the redox shuttle capacity of the liver and possibly it could also replace citrin as an aspartate provider for arginine succinate synthetase 1 (ASS1) and the urea cycle, although this remains to be established. As therapy with hCitrin may give rise to immune reactions in patients lacking CITRIN protein, and ARALAR protein is already present in these patients, the use of a hAralar-based therapy is not expected to trigger immune problems and could result in a safe way to treat the condition.

Table 1
Comparison between Mouse and Human liver redox shuttle components. Data correspond to published label-free quantification proteomics from mouse [49] or human [50] hepatocytes, or from absolute quantification with AQUA peptides of whole liver mitochondria (this study).

	Method	Source	Mouse liver	Human liver
Citrin/ Aralar	Relative quantification Free-label proteomics	Mouse: [49] Human: [50]	~ 10.5	~ 3802
Citrin/ GPD2			~ 6.2	~ 535
Citrin/ Aralar	Abstolute quantification (AQUA peptides)	(this study)	~ 7.8	~ 397

5. Limitations of study/ additional considerations

From a methodological point of view, it should be pointed out that reconstitution of MAS activity in mouse liver mitochondria is not exclusively dependent on aralar and citrin. Basal MAS activity, i.e., that observed in *citrin (−/−)* mitochondria is larger than that attributed to endogenous liver aralar and larger than that observed in mouse brain mitochondria from *aralar (−/−)* mice [8] which lack the major brain AGC. This opens up the possibility that other transport systems that have been proposed as mitochondrial aspartate [61,62] or glutamate (Slc25a22, Slc25a18 [63]) carriers may contribute to the activity of the reconstituted system. Further work will be required to clarify this issue.

Conflict of interest statement

Authors declare no competing interests.

Data availability

Data will be made available on request.

Acknowledgements

This work was supported by the CITRIN FOUNDATION, in Singapore founded by Barbara Yu Fa and Yen How Tai (to J.S.), by MICINN [grant PID2020-114499RB-I00 AEI/FEDER, UE, to A. del A.], by Instituto de Investigación Hospital 12 de Octubre (Imas12), Madrid, Spain [grant 2019/0039 to M.P.-C.] by Ministerio de Ciencia, Innovación y Universidades MICINN [grant PID2020-117116RB-I00 in "Plan Estatal de Investigación Cientifica y Técnica y Innovación, cofinanciado con Fondos FEDER (to M.L.M.-C.]; by La Caixa Foundation Program (to M.L.M.-C.), by Programa Retos [RTC2019-007125-1, to M.L.M.-C.)], Proyectos Investigacion en Salud [DTS20/00138 to M.L.M.-C.], and by institutional grant from Fundación Areces to the Centro de Biología Molecular Severo Ochoa. L.G.-M. was recipient of predoctoral fellowship from MINECO and A.S.-C. was recipient of a predoctoral research contract from Comunidad de Madrid. We thank Bárbara Sesé, Beatriz García, and Pilar del Hoyo for excellent technical assistance, Belén Pintado and Verónica Domínguez for discussion and assistance on transgenic mice generation; and Optical and Confocal Microscopy unit (SMOC) of the CBMSO for their support.

Appendix A. Supplementary data

Supplementary data to this article can be found online at https://doi.org/10.1016/j.ymgmr.2023.100967.

References

[1] J. Satrústegui, B. Pardo, A. del Arco, Mitochondrial transporters as novel targets for intracellular calcium signaling, Physiol. Rev. 87 (2007) 29–67, https://doi.org/10.1152/physrev.00005.2006.

[2] L. Palmieri, B. Pardo, F.M. Lasorsa, A. del Arco, K. Kobayashi, M. Iijima, M. J. Runswick, J.E. Walker, T. Saheki, J. Satrústegui, F. Palmieri, Citrin and aralar1 are Ca(2+)-stimulated aspartate/glutamate transporters in mitochondria, EMBO J. 20 (2001) 5060–5069, https://doi.org/10.1093/emboj/20.18.5060.

[3] A. del Arco, J. Satrústegui, Molecular cloning of Aralar, a new member of the mitochondrial carrier superfamily that binds calcium and is present in human muscle and brain, J. Biol. Chem. 273 (1998) 23327–23334, https://doi.org/10.1074/jbc.273.36.23327.

[4] K. Kobayashi, D.S. Sinasac, M. Iijima, A.P. Boright, L. Begum, J.R. Lee, T. Yasuda, S. Ikeda, R. Hirano, H. Terazono, M.A. Crackower, I. Kondo, L.-C. Tsui, S. W. Scherer, T. Saheki, The gene mutated in adult-onset type II citrullinaemia encodes a putative mitochondrial carrier protein, Nat. Genet. 22 (1999) 159–163, https://doi.org/10.1038/9667.

[5] A. Del Arco, M. Agudo, J. Satrústegui, Characterization of a second member of the subfamily of calcium-binding mitochondrial carriers expressed in human non-excitable tissues, Biochem. J. 345 (Pt 3) (2000) 725–732, https://doi.org/10.1042/0264-6021:3450725.

[6] P. Borst, The malate-aspartate shuttle (Borst cycle): how it started and developed into a major metabolic pathway, IUBMB Life 72 (2020) 2241–2259, https://doi.org/10.1002/iub.2367.

[7] L.B. Sullivan, D.Y. Gui, A.M. Hosios, L.N. Bush, E. Freinkman, M.G. Vander Heiden, Supporting aspartate biosynthesis is an essential function of respiration in proliferating cells, Cell. 162 (2015) 552–563, https://doi.org/10.1016/j.cell.2015.07.017.

[8] M.A. Jalil, L. Begum, L. Contreras, B. Pardo, M. Iijima, M.X. Li, M. Ramos, P. Marmol, M. Horiuchi, K. Shimotsu, S. Nakagawa, A. Okubo, M. Sameshima, Y. Isashiki, A. Del Arco, K. Kobayashi, J. Satrústegui, T. Saheki, Reduced N-acetylaspartate levels in mice lacking aralar, a brain- and muscle-type mitochondrial aspartate-glutamate carrier, J. Biol. Chem. 280 (2005) 31333–31339, https://doi.org/10.1074/jbc.M505286200.

[9] B. Pardo, T.B. Rodrigues, L. Contreras, M. Garzón, I. Llorente-Folch, K. Kobayashi, T. Saheki, S. Cerdan, J. Satrústegui, Brain glutamine synthesis requires neuronal-born aspartate as amino donor for glial glutamate formation, J. Cereb. Blood Flow Metab. Off. J. Int. Soc. Cereb. Blood Flow Metab. 31 (2011) 90–101, https://doi.org/10.1038/jcbfm.2010.146.

[10] T. Saheki, M. Moriyama, A. Funahashi, E. Kuroda, AGC2 (citrin) deficiency-from recognition of the disease till construction of therapeutic procedures, Biomolecules. 10 (2020) E1100, https://doi.org/10.3390/biom10081100.

[11] A. del Arco, J. Morcillo, J.R. Martínez-Morales, C. Galián, V. Martos, P. Bovolenta, J. Satrústegui, Expression of the aspartate/glutamate mitochondrial carriers aralar1 and citrin during development and in adult rat tissues, Eur. J. Biochem. 269 (2002) 3313–3320, https://doi.org/10.1046/j.1432-1033.2002.03018.x.

[12] M. Ramos, A. del Arco, B. Pardo, A. Martínez-Serrano, J.R. Martínez-Morales, K. Kobayashi, T. Yasuda, E. Bogónez, P. Bovolenta, T. Saheki, J. Satrústegui, Developmental changes in the Ca2+−regulated mitochondrial aspartate-glutamate carrier aralar1 in brain and prominent expression in the spinal cord, Brain Res. Dev. Brain Res. 143 (2003) 33–46, https://doi.org/10.1016/s0165-3806(03)00097-x.

[13] M. Iijima, A. Jalil, L. Begum, T. Yasuda, N. Yamaguchi, M. Xian Li, N. Kawada, H. Endou, K. Kobayashi, T. Saheki, Pathogenesis of adult-onset type II citrullinemia caused by deficiency of citrin, a mitochondrial solute carrier protein: tissue and subcellular localization of citrin, Adv. Enzym. Regul. 41 (2001) 325–342, https://doi.org/10.1016/S0065-2571(00)00022-4.

[14] T. Saheki, K. Kobayashi, M. Iijima, M. Moriyama, M. Yazaki, Y. Takei, S. Ikeda, Metabolic derangements in deficiency of citrin, a liver-type mitochondrial aspartate–glutamate carrier, Hepatol. Res. (2005) 4, https://doi.org/10.1016/j.hepres.2005.09.031.

[15] Y. Okano, Current treatment for citrin deficiency during NICCD and adaptation/compensation stages_ strategy to prevent CTLN2, Mol. Genet. Metab. 127 (2019) 175–183.

[16] J. Kido, J. Häberle, K. Sugawara, T. Tanaka, M. Nagao, T. Sawada, Y. Wada, C. Numakura, K. Murayama, Y. Watanabe, K. Kojima-Ishii, H. Sasai, K. Kosugiyama, K. Nakamura, Clinical manifestation and long-term outcome of citrin deficiency: report from a nationwide study in Japan, J. Inherit. Metab. Dis. (2022), https://doi.org/10.1002/jimd.12483 jimd.12483.

[17] T. Saheki, K. Inoue, A. Tushima, K. Mutoh, K. Kobayashi, Citrin deficiency and current treatment concepts, Mol. Genet. Metab. 6 (2010).

[18] L. Bočkor, G. Bortolussi, A. Iaconcig, G. Chiaruttini, C. Tiribelli, M. Giacca, F. Benvenuti, L. Zentilin, A.F. Muro, Repeated AAV-mediated gene transfer by serotype switching enables long-lasting therapeutic levels of hUgt1a1 enzyme in a mouse model of Crigler-Najjar syndrome type I, Gene Ther. 24 (2017) 649–660, https://doi.org/10.1038/gt.2017.75.

[19] F.D. Ledley, H.E. Grenett, A.G. DiLella, S.C. Kwok, S.L. Woo, Gene transfer and expression of human phenylalanine hydroxylase, Science. 228 (1985) 77–79, https://doi.org/10.1126/science.3856322.

[20] G. Gonzalez-Aseguinolaza, J. Prieto, Gene therapy of liver diseases: A 2011 perspective, Clin. Res. Hepatol. Gastroenterol. 35 (2011) 699–708, https://doi.org/10.1016/j.clinre.2011.05.016.

[21] O. Cao, Impact of the underlying mutation and the route of vector administration on immune responses to factor IX in gene therapy for hemophilia B, Cell Ther. 17 (2009) 10.

[22] O. Murillo, D.M. Luqui, C. Gazquez, D. Martinez-Espartosa, I. Navarro-Blasco, J. I. Monreal, L. Guembe, A. Moreno-Cermeño, F.J. Corrales, J. Prieto, R. Hernandez-Alcoceba, G. Gonzalez-Aseguinolaza, Long-term metabolic correction of Wilson's disease in a murine model by gene therapy, J. Hepatol. 64 (2016) 419–426, https://doi.org/10.1016/j.jhep.2015.09.014.

[23] S. Tavoulari, D. Lacabanne, C. Thangaratnarajah, E.R.S. Kunji, Pathogenic variants of the mitochondrial aspartate/glutamate carrier causing citrin deficiency, Trends Endocrinol Metab 33 (2022) 539–553, https://doi.org/10.1016/j.tem.2022.05.002.

[24] H.-Y. Fu, S.-R. Zhang, X.-H. Wang, T. Saheki, K. Kobayashi, J.-S. Wang, The mutation spectrum of the SLC25A13 gene in Chinese infants with intrahepatic cholestasis and aminoacidemia, J. Gastroenterol. 46 (2011) 510–518, https://doi.org/10.1007/s00535-010-0329-y.

[25] T. Yasuda, N. Yamaguchi, K. Kobayashi, I. Nishi, H. Horinouchi, Md.A. Jalil, M. X. Li, M. Ushikai, M. Iijima, I. Kondo, T. Saheki, Identification of two novel mutations in the SLC25A13 gene and detection of seven mutations in 102 patients with adult-onset type II citrullinemia, Hum. Genet. 107 (2000) 537–545, https://doi.org/10.1007/s004390000430.

[26] R. Ferla, P. Claudiani, M. Savarese, K. Kozarsky, R. Parini, M. Scarpa, M.A. Donati, G. Sorge, J.J. Hopwood, G. Parenti, S. Fecarotta, V. Nigro, H.S. Sivri, A. Van Der Ploeg, G. Andria, N. Brunetti-Pierri, A. Auricchio, Prevalence of anti–adeno-associated virus serotype 8 neutralizing antibodies and arylsulfatase B cross-

reactive immunologic material in Mucopolysaccharidosis VI patient candidates for a gene therapy trial, Hum. Gene Ther. 26 (2015) 145–152, https://doi.org/10.1089/hum.2014.109.
[27] J.R. Mendell, Z. Sahenk, D. Bowles, G. Galloway, K.R. Clark, S.W. McPhee, C. M. Walker, Dystrophin immunity in Duchenne's muscular dystrophy, N. Engl. J. Med. 9 (2010).
[28] L. Contreras, P. Gomez-Puertas, M. Iijima, K. Kobayashi, T. Saheki, J. Satrústegui, Ca2+ activation kinetics of the two aspartate-glutamate mitochondrial carriers, aralar and citrin: role in the heart malate-aspartate NADH shuttle, J. Biol. Chem. 282 (2007) 7098–7106, https://doi.org/10.1074/jbc.M610491200.
[29] M.G. Kramer, In vitro and in vivo comparative study of chimeric liver-specific promoters 7, 2003, p. 11.
[30] T. Choi, M. Huang, C. Gorman, R. Jaenisch, A generic intron increases gene expression in transgenic mice, Mol. Cell. Biol. 11 (1991) 3070–3074, https://doi.org/10.1128/mcb.11.6.3070-3074.1991.
[31] A.J. Clark, A.L. Archibald, M. McClenaghan, J.P. Simons, R. Wallace, C. B. Whitelaw, Enhancing the efficiency of transgene expression, Philos. Trans. R. Soc. Lond. Ser. B Biol. Sci. 339 (1993) 225–232, https://doi.org/10.1098/rstb.1993.0020.
[32] B.P. Duncker, P.L. Davies, V.K. Walker, Introns boost transgene expression in Drosophila melanogaster, Mol. Gen. Genet. MGG 254 (1997) 291–296, https://doi.org/10.1007/s004380050418.
[33] L. Contreras, A. Urbieta, K. Kobayashi, T. Saheki, J. Satrústegui, Low levels of citrin (*SLC25A13*) expression in adult mouse brain restricted to neuronal clusters: citrin expression in the brain, J. Neurosci. Res. 88 (2010) 1009–1016, https://doi.org/10.1002/jnr.22283.
[34] N. Goikoetxea-Usandizaga, M. Serrano-Maciá, T.C. Delgado, J. Simón, D. Fernández Ramos, D. Barriales, M.E. Cornide, M. Jiménez, M. Pérez-Redondo, S. Lachiondo-Ortega, R. Rodríguez-Agudo, M. Bizkarguenaga, J.D. Zalamea, S. T. Pasco, D. Caballero-Díaz, B. Alfano, M. Bravo, I. González-Recio, M. Mercado-Gómez, C. Gil-Pitarch, J. Mabe, J. Gracia-Sancho, L. Abecia, Ó. Lorenzo, P. Martín-Sanz, N.G.A. Abrescia, G. Sabio, M. Rincón, J. Anguita, E. Miñambres, C. Martín, M. Berenguer, I. Fabregat, M. Casado, C. Peralta, M. Varela-Rey, M.L. Martínez-Chantar, Mitochondrial bioenergetics boost macrophage activation, promoting liver regeneration in metabolically compromised animals, Hepatology. 75 (2022) 550–566, https://doi.org/10.1002/hep.32149.
[35] L. Contreras, J. Satrústegui, Calcium signaling in brain mitochondria: interplay of malate aspartate NADH shuttle and calcium uniporter/mitochondrial dehydrogenase pathways, J. Biol. Chem. 284 (2009) 7091–7099, https://doi.org/10.1074/jbc.M808066200.
[36] J.M. Cuezva, M. Krajewska, M.L. de Heredia, S. Krajewski, G. Santamaría, H. Kim, J.M. Zapata, H. Marusawa, M. Chamorro, J.C. Reed, The bioenergetic signature of cancer: a marker of tumor progression, Cancer Res. 62 (2002) 6674–6681.
[37] Y.P. Hung, G. Yellen, Live-cell imaging of cytosolic NADH–NAD+ redox state using a genetically encoded fluorescent biosensor, in: J. Zhang, Q. Ni, R.H. Newman (Eds.), Fluoresc. Protein-Based Biosens, Humana Press, Totowa, NJ, 2014, pp. 83–95, https://doi.org/10.1007/978-1-62703-622-1_7.
[38] Y.P. Hung, J.G. Albeck, M. Tantama, G. Yellen, Imaging cytosolic NADH-NAD+ redox state with a genetically encoded fluorescent biosensor, Cell Metab. 14 (2011) 545–554, https://doi.org/10.1016/j.cmet.2011.08.012.
[39] M. Tantama, J.R. Martínez-François, R. Mongeon, G. Yellen, Imaging energy status in live cells with a fluorescent biosensor of the intracellular ATP-to-ADP ratio, Nat. Commun. 4 (2013) 2550, https://doi.org/10.1038/ncomms3550.
[40] A. Guarás, E. Perales-Clemente, E. Calvo, R. Acín-Pérez, M. Loureiro-Lopez, C. Pujol, I. Martínez-Carrascoso, E. Nuñez, F. García-Marqués, M.A. Rodríguez-Hernández, A. Cortés, F. Diaz, A. Pérez-Martos, C.T. Moraes, P. Fernández-Silva, A. Trifunovic, P. Navas, J. Vazquez, J.A. Enríquez, The CoQH2/CoQ ratio serves as a sensor of respiratory chain efficiency, Cell Rep. 15 (2016) 197–209, https://doi.org/10.1016/j.celrep.2016.03.009.
[41] B. MacLean, D.M. Tomazela, N. Shulman, M. Chambers, G.L. Finney, B. Frewen, R. Kern, D.L. Tabb, D.C. Liebler, M.J. MacCoss, Skyline: an open source document editor for creating and analyzing targeted proteomics experiments, Bioinformatics. 26 (2010) 966–968, https://doi.org/10.1093/bioinformatics/btq054.
[42] D.S. Sinasac, M. Moriyama, M.A. Jalil, L. Begum, M.X. Li, M. Iijima, M. Horiuchi, B. H. Robinson, K. Kobayashi, T. Saheki, L.-C. Tsui, *Slc25a13* -knockout mice harbor metabolic deficits but fail to display hallmarks of adult-onset type II Citrullinemia, Mol. Cell. Biol. 24 (2004) 527–536, https://doi.org/10.1128/MCB.24.2.527-536.2004.
[43] Z. Koshenov, F.E. Oflaz, M. Hirtl, B. Gottschalk, R. Rost, R. Malli, W.F. Graier, Citrin mediated metabolic rewiring in response to altered basal subcellular Ca2+ homeostasis, Commun. Biol. 5 (2022) 76, https://doi.org/10.1038/s42003-022-03019-2.
[44] G. Puertas-Frías, A. del Arco, B. Pardo, J. Satrústegui, L. Contreras, Mitochondrial movement in Aralar/Slc25a12/AGC1 deficient cortical neurons, Neurochem. Int. 131 (2019), 104541, https://doi.org/10.1016/j.neuint.2019.104541.
[45] L.E. Dow, Z. Nasr, M. Saborowski, S.H. Ebbesen, E. Manchado, N. Tasdemir, T. Lee, J. Pelletier, S.W. Lowe, Conditional reverse tet-transactivator mouse strains for the efficient induction of TRE-regulated transgenes in mice, PLoS One 9 (2014), e95236, https://doi.org/10.1371/journal.pone.0095236.
[46] S. Kanzler, A.W. Lohse, A. Keil, J. Henninger, H.P. Dienes, P. Schirmacher, S. Rose-John, K.H. Meyer Zum Büschenfelde, M. Blessing, TGF-β1 in liver fibrosis: an inducible transgenic mouse model to study liver fibrogenesis, Am. J. Physiol.-Gastrointest. Liver Physiol. 276 (1999) G1059–G1068, https://doi.org/10.1152/ajpgi.1999.276.4.G1059.
[47] Y. Zhang, S.-Z. Huang, S. Wang, Y.-T. Zeng, Development of an HSV-tk transgenic mouse model for study of liver damage: development of an HSV-tk transgenic mouse model, FEBS J. 272 (2005) 2207–2215, https://doi.org/10.1111/j.1742-4658.2005.04644.x.
[48] O. Argyros, S.P. Wong, M. Niceta, S.N. Waddington, S.J. Howe, C. Coutelle, A. D. Miller, R.P. Harbottle, Persistent episomal transgene expression in liver following delivery of a scaffold/matrix attachment region containing non-viral vector, Gene Ther. 15 (2008) 1593–1605, https://doi.org/10.1038/gt.2008.113.
[49] S.B. Azimifar, N. Nagaraj, J. Cox, M. Mann, Cell-type-resolved quantitative proteomics of murine liver, Cell Metab. 20 (2014) 1076–1087, https://doi.org/10.1016/j.cmet.2014.11.002.
[50] M. Ölander, J.R. Wiśniewski, P. Artursson, Cell-type-resolved proteomic analysis of the human liver, Liver Int. 40 (2020) 1770–1780, https://doi.org/10.1111/liv.14452.
[51] J. Cao, D. An, M. Galduroz, J. Zhuo, S. Liang, M. Eybye, A. Frassetto, E. Kuroda, A. Funahashi, J. Santana, C. Mihai, K.E. Benenato, E.S. Kumarasinghe, S. Sabnis, T. Salerno, K. Coughlan, E.J. Miracco, B. Levy, G. Besin, J. Schultz, C. Lukacs, L. Guey, P. Finn, T. Furukawa, P.H. Giangrande, T. Saheki, P.G.V. Martini, mRNA therapy improves metabolic and behavioral abnormalities in a murine model of citrin deficiency, Mol. Ther. J. Am. Soc. Gene Ther. 27 (2019) 1242–1251, https://doi.org/10.1016/j.ymthe.2019.04.017.
[52] T. Saheki, M. Iijima, M.X. Li, K. Kobayashi, M. Horiuchi, M. Ushikai, F. Okumura, X.J. Meng, I. Inoue, A. Tajima, M. Moriyama, K. Eto, T. Kadowaki, D.S. Sinasac, L.-C. Tsui, M. Tsuji, A. Okano, T. Kobayashi, Citrin/mitochondrial glycerol-3-phosphate dehydrogenase double knock-out mice recapitulate features of human citrin deficiency, J. Biol. Chem. 282 (2007) 25041–25052, https://doi.org/10.1074/jbc.M702031200.
[53] P. Berraondo, P.G.V. Martini, M.A. Avila, A. Fontanellas, Messenger RNA therapy for rare genetic metabolic diseases, Gut. 68 (2019) 1323–1330, https://doi.org/10.1136/gutjnl-2019-318269.
[54] J.S. Lee, L. Adler, H. Karathia, N. Carmel, S. Rabinovich, N. Auslander, R. Keshet, N. Stettner, A. Silberman, L. Agemy, D. Helbling, R. Eilam, Q. Sun, A. Brandis, S. Malitsky, M. Itkin, H. Weiss, S. Pinto, S. Kalaora, R. Levy, E. Barnea, A. Admon, D. Dimmock, N. Stern-Ginossar, A. Scherz, S.C.S. Nagamani, M. Unda, D.M. Wilson, R. Elhasid, A. Carracedo, Y. Samuels, S. Hannenhalli, E. Ruppin, A. Erez, Urea cycle dysregulation generates clinically relevant genomic and biochemical signatures, Cell. 174 (2018) 1559–1570.e22, https://doi.org/10.1016/j.cell.2018.07.019.
[55] S. Rabinovich, A. Silberman, L. Adler, S. Agron, S. Levin-Zaidman, A. Bahat, Z. Porat, E. Ben-Zeev, I. Geva, M. Itkin, S. Malitsky, A. Buchaklian, D. Helbling, D. Dimmock, A. Erez, The mitochondrial carrier citrin plays a role in regulating cellular energy during carcinogenesis, Oncogene. 39 (2020) 164–175, https://doi.org/10.1038/s41388-019-0976-2.
[56] E. Hajaj, M. Sciacovelli, C. Frezza, A. Erez, The context-specific roles of urea cycle enzymes in tumorigenesis, Mol. Cell 81 (2021) 3749–3759, https://doi.org/10.1016/j.molcel.2021.08.005.
[57] V. Infantino, F. Dituri, P. Convertini, A. Santarsiero, F. Palmieri, S. Todisco, S. Mancarella, G. Giannelli, V. Iacobazzi, Epigenetic upregulation and functional role of the mitochondrial aspartate/glutamate carrier isoform 1 in hepatocellular carcinoma, Biochim. Biophys. Acta (BBA) - Mol. Basis Dis. 1865 (2019) 38–47, https://doi.org/10.1016/j.bbadis.2018.10.018.
[58] H.C.D. Medeiros, S.Y. Lunt, The Warburg effect: saturation of mitochondrial NADH shuttles triggers aerobic lactate fermentation, Mol. Cell 82 (2022) 3119–3121, https://doi.org/10.1016/j.molcel.2022.08.004.
[59] Y. Wang, E. Stancliffe, R. Fowle-Grider, R. Wang, C. Wang, M. Schwaiger-Haber, L. P. Shriver, G.J. Patti, Saturation of the mitochondrial NADH shuttles drives aerobic glycolysis in proliferating cells, Mol. Cell 82 (2022) 3270–3283.e9, https://doi.org/10.1016/j.molcel.2022.07.007.
[60] A. Luengo, Z. Li, D.Y. Gui, L.B. Sullivan, M. Zagorulya, B.T. Do, R. Ferreira, A. Naamati, A. Ali, C.A. Lewis, C.J. Thomas, S. Spranger, N.J. Matheson, M. G. Vander Heiden, Increased demand for NAD+ relative to ATP drives aerobic glycolysis, Mol. Cell 81 (2021) 691–707.e6, https://doi.org/10.1016/j.molcel.2020.12.012.
[61] A. Vozza, G. Parisi, F. De Leonardis, F.M. Lasorsa, A. Castegna, D. Amorese, R. Marmo, V.M. Calcagnile, L. Palmieri, D. Ricquier, E. Paradies, P. Scarcia, F. Palmieri, F. Bouillaud, G. Fiermonte, UCP2 transports C4 metabolites out of mitochondria, regulating glucose and glutamine oxidation, Proc. Natl. Acad. Sci. 111 (2014) 960–965, https://doi.org/10.1073/pnas.1317400111.
[62] S. Raho, L. Capobianco, R. Malivindi, A. Vozza, C. Piazzolla, F. De Leonardis, R. Gorgoglione, P. Scarcia, F. Pezzuto, G. Agrimi, S.N. Barile, I. Pisano, S. J. Reshkin, M.R. Greco, R.A. Cardone, V. Rago, Y. Li, C.M.T. Marobbio, W. Sommergruber, C.L. Riley, F.M. Lasorsa, E. Mills, M.C. Vegliante, G.E. De Benedetto, D. Fratantonio, L. Palmieri, V. Dolce, G. Fiermonte, KRAS-regulated glutamine metabolism requires UCP2-mediated aspartate transport to support pancreatic cancer growth, Nat. Metab. 2 (2020) 1373–1381, https://doi.org/10.1038/s42255-020-00315-1.
[63] G. Fiermonte, L. Palmieri, S. Todisco, G. Agrimi, F. Palmieri, J.E. Walker, Identification of the mitochondrial glutamate transporter, J. Biol. Chem. 277 (2002) 19289–19294, https://doi.org/10.1074/jbc.M201572200.